# Numerical Analysis of Isothermal Gaseous Flows in Microchannel

By *Bin Cao*, *Guangwen Chen*, *Ying Li*, and *Quan Yuan**

**DOI:** 10.1002/ceat.200407079

Two-dimensional compressible momentum equations were solved by a perturbation analysis and the PISO algorithm to investigate the effects of compressibility and rarefaction on the local flow resistance of isothermal gas flow in circular microchannels. The computations were performed for a wide range of Reynolds numbers and inlet Mach numbers. The explicit expression of the normalized local Fanning friction factor along the microchannel was derived in the present paper. The results reveal that the local Fanning friction factor is a function of the inlet Mach number, the Reynolds number and the length-diameter ratio of the channel. For larger Reynolds and inlet Mach numbers, the friction coefficient in the microchannel is higher than the value in a macrotube, and the gas flow in the microchannel is dominated only by compressibility. For smaller Reynolds and inlet Mach numbers, the Fanning friction factor of gas flow in the microchannel is lower than that in a circular tube of conventional size due to slip flow at the wall and thus, rarefaction has a significant effect on the fluid flow characteristics in a microchannel.

## 1 Introduction

The rapid development of microchemical (MCS) and microelectromechanic systems (MEMS) has brought up a great interest in understanding the characteristics of flow and heat transfer at a micro scale in the past two decades.

Wu and Little [1] measured the friction factors of nitrogen, argon and helium flow in microchannels with hydraulic diameters ranging from 45.46 to 83.08 μm. They found that these friction factors were much larger than the predictions by the classic theory for laminar flow in conventional channels. Guo and Wu [2] numerically solved the governing equations for compressible flow in a microtube. The results of their calculation showed that the effect of compressibility is important for gaseous flow in microtubes, which causes that the friction coefficients along the tube are larger than the values in a conventional size tube and are no longer constant.

However, Pfahler et al. [3,4] found that for microchannels with hydraulic diameters of 0.98–39.7 μm, the friction factors were lower than those predicted by the classic theory. For a small Reynolds number, the friction constant tends to increase with increasing Reynolds numbers. Choi et al. [5] investigated the flow resistance of nitrogen gas flow in microtubes with hydraulic diameters between 3 and 81 μm and found that the measured friction factors were smaller than those predicted by the classic theory.

Kavehpour et al. [6] and Chen et al. [7] studied the effects of compressibility and rarefaction on gaseous flows in mcirochannels. Two-dimensional compressible forms of momentum and energy equations were solved with slip velocity and temperature jump boundary conditions in a parallel plate microchannel. The numerical results revealed that the Nusselt number and the friction coefficient were substantially reduced for slip flows compared with the continuum flows.

As can be seen above, there are inconsistencies in the results of experimental and numerical analyses reported by different researchers. Thus, the motivation of this paper is to numerically analyze the effects of compressibility and rarefaction on the local flow resistance of gas flow in circular microchannels for a wide range of operating conditions.

## 2 Analysis

### 2.1 Governing Equations and Numerical Calculation

The isothermal flow of an ideal gas in a circular microchannel is considered. For the laminar steady-state flow, the two-dimensional compressible Navier-Stokes equations expressed in cylindrical coordinate take the following forms:

Continuity:

$$\frac{\partial(\rho u)}{\partial x} + \frac{1}{r}\frac{\partial(\rho r v)}{\partial r} = 0 \tag{1}$$

Momentum:

$$\frac{\partial(\rho u u)}{\partial x} + \frac{1}{r}\frac{\partial(\rho v r u)}{\partial r} = -\frac{\partial P}{\partial x} + \frac{\partial}{\partial x}\left(\mu\frac{\partial u}{\partial x}\right) + \frac{1}{r}\frac{\partial}{\partial r}\left(\mu r\frac{\partial u}{\partial r}\right) + S_u \tag{2}$$

$$\frac{\partial(\rho u v)}{\partial x} + \frac{1}{r}\frac{\partial(\rho v r v)}{\partial r} = -\frac{\partial P}{\partial r} + \frac{\partial}{\partial x}\left(\mu\frac{\partial v}{\partial x}\right) + \frac{1}{r}\frac{\partial}{\partial r}\left(\mu r\frac{\partial v}{\partial r}\right) - \mu\frac{v}{r^2} + S_v \tag{3}$$

[*] Dr. B. Cao, G. Chen, Y. Li, Prof. Q. Yuan (qyuan@dcip.ac.cn), Dalian Institute of Chemical Physics, Chinese Academy of Sciences, 457 Zhongshan Road, Dalian 116023, PR China.

where

$$S_u = \frac{\mu}{3}\frac{\partial}{\partial x}\left(\frac{\partial u}{\partial x} + \frac{1}{r}\frac{\partial (rv)}{\partial r}\right) \qquad S_v = \frac{\mu}{3}\frac{\partial}{\partial r}\left(\frac{\partial u}{\partial x} + \frac{1}{r}\frac{\partial (rv)}{\partial r}\right) \quad (4)$$

In the present paper, the terms $S_u$ and $S_v$ can be omitted in the momentum equation because they are less important than the other terms.

The equation of state for ideal gas is

$$P = \frac{\rho}{M} R_g T \quad (5)$$

The initial and boundary conditions are

$$x = 0, \quad u = 2\bar{u}_{in}\left(1 - \left(\frac{r}{R_0}\right)^2\right), \qquad v = 0 \quad (6)$$

$$x > 0, \qquad r = 0, \qquad \frac{\partial u}{\partial r} = 0, \qquad v = 0 \quad (7)$$

The first-order slip velocity boundary conditions are expressed as

$$r = R_0, \qquad u|_{wall} = -\frac{2 - \sigma_v}{\sigma_v}\lambda \left.\frac{\partial u}{\partial r}\right|_{r=R_0}, \qquad v = 0 \quad (8)$$

where $\sigma_v$ is the tangential momentum accommodation coefficient. This coefficient indicates the influence of rarefaction and fluid-surface interaction. It is thought to vary between 0 and 1 depending on the surface roughness, temperature and gas type. Here, $\sigma_v = 1$ [8].

The Fanning friction factor for the isothermal compressible flow is defined as [9]

$$f_F = \frac{\tau_W}{1/2\bar{\rho}\bar{u}^2} = \frac{D_h}{2\bar{P}}\left(\frac{d\bar{P}}{dx}\right) - \frac{D_h}{2\bar{\rho}\bar{u}^2}\left(\frac{d\bar{P}}{dx}\right) \quad (9)$$

For fully developed incompressible laminar no-slip flow in a circular tube, the Fanning friction factor is 16/Re, so the normalized Fanning friction factor (or coefficient) can be expressed as

$$NC_F = \frac{f_F}{16/\mathrm{Re}} \quad (10)$$

The governing equation of nitrogen flow was solved by a control volume finite-difference scheme and the PISO (pressure implicit split operator) algorithm [10]. The power law scheme was applied to discredit the convective terms in the moment equation. A grid dependence test using a 60 (radial) × 400 (axial) uniform staggered grid was performed for the numerical calculation in this study. A line-by-line method was employed to solve the resulting algebraic equations. Alternating sweeps of tridiagonal matrix algorithm combined with a block correction were applied to each variable. The ratio of channel length to diameter was set to be 400. Nitrogen was used as working fluid in the calculation $\gamma$ = 1.4).

**2.2 Perturbation Analysis of Governing Equations at Low Reynolds and Mach Number**

Arkilic et al. [8] used a perturbation method to analytically solve two-dimensional Navier-Stokes equations with first-order slip boundary conditions for a compressible gas flow in parallel plane microchannels. In this paper, their procedure is followed to investigate the compressible gas flow in circular microchannels, but with a different method in solving the continuity equation and pressure distribution.

The following dimensionless variables are used:

$$\tilde{P} = \frac{P}{P_{in}}, \tilde{\rho} = \frac{\rho}{\rho_{in}}, \tilde{u} = \frac{u}{\bar{u}_{in}}, \tilde{v} = \frac{v}{\bar{u}_{in}}, \tilde{x} = \frac{x}{L}, \tilde{r} = \frac{r}{R_0}, \varepsilon = \frac{R_0}{L}$$

The governing equations can be expressed as

$$\varepsilon\frac{\partial(\tilde{\rho}\tilde{u})}{\partial\tilde{x}} + \frac{1}{\tilde{r}}\frac{\partial(\tilde{\rho}\tilde{r}\tilde{v})}{\partial\tilde{r}} = 0 \quad (11)$$

$$\frac{\mathrm{Re}}{2}\left(\varepsilon\frac{\partial(\tilde{\rho}\tilde{u}\tilde{u})}{\partial\tilde{x}} + \frac{1}{\tilde{r}}\frac{\partial(\tilde{\rho}\tilde{r}\tilde{u}\tilde{v})}{\partial\tilde{r}}\right) = -\frac{\varepsilon\,\mathrm{Re}}{2\gamma Ma_{in}^2}\frac{\partial\tilde{P}}{\partial\tilde{x}} + \varepsilon^2\frac{\partial^2\tilde{u}}{\partial\tilde{x}^2} + \frac{1}{\tilde{r}}\frac{\partial}{\partial\tilde{r}}\left(\tilde{r}\frac{\partial\tilde{u}}{\partial\tilde{r}}\right) \quad (12)$$

$$\frac{\mathrm{Re}}{2}\left(\varepsilon\frac{\partial(\tilde{\rho}\tilde{u}\tilde{v})}{\partial\tilde{x}} + \frac{1}{\tilde{r}}\frac{\partial(\tilde{\rho}\tilde{r}\tilde{v}\tilde{v})}{\partial\tilde{r}}\right) = -\frac{\mathrm{Re}}{2\gamma Ma_{in}^2}\frac{\partial\tilde{P}}{\partial\tilde{r}} + \varepsilon^2\frac{\partial^2\tilde{v}}{\partial\tilde{x}^2} + \frac{1}{\tilde{r}}\frac{\partial}{\partial\tilde{r}}\left(\tilde{r}\frac{\partial\tilde{v}}{\partial\tilde{r}}\right) - \frac{\tilde{v}}{\tilde{r}^2} \quad (13)$$

$$\tilde{x} = 0, \qquad \tilde{u} = 2(1 - \tilde{r}^2), \qquad \tilde{v} = 0 \quad (14)$$

$$\tilde{x} > 0, \qquad \tilde{r} = 0, \qquad \frac{\partial\tilde{u}}{\partial\tilde{r}} = 0, \qquad \tilde{v} = 0 \quad (15)$$

$$\tilde{r} = 1, \qquad \tilde{u}|_{\tilde{r}=1} = -2\frac{2 - \sigma_v}{\sigma_v}Kn\left.\frac{\partial\tilde{u}}{\partial\tilde{r}}\right|_{\tilde{r}=1}, \qquad \tilde{v} = 0 \quad (16)$$

$$\mathrm{Re} = \frac{D_h\bar{u}_{in}\rho_{in}}{\mu}, Ma_{in} = \frac{\bar{u}_{in}}{\sqrt{\gamma R_g T/M}}, \qquad Kn = \frac{Kn_{in}}{\tilde{P}_0}, \qquad Kn_{in} = \sqrt{\frac{\pi\gamma}{2}}\frac{Ma_{in}}{\mathrm{Re}} \quad (17)$$

Utilizing a perturbation analysis and considering $\varepsilon << 1$, $Re \sim O(\varepsilon)$, $Ma_{in} \sim O(\varepsilon)$, $\gamma\, Ma_{in}^2/Re \sim O(\varepsilon)$, the following equation can be obtained from the $\tilde{r}$momentum equation,

$$\tilde{P}_0 = \tilde{P}_0(x) \quad (18)$$

where the subscript '0' denotes the zero order variables in perturbation expansion. Substituting the above equation into the continuity equation (11), multiplying Eq. (11) by $2\pi\,\tilde{r}$ and integrating once with respect to $\tilde{r}$, and then multiplying it by $1/\pi\, R_0^2$, one can obtain

$$\tilde{P}_0\bar{\tilde{u}}_0 = 1 \quad (19)$$

  

The $\tilde{x}$ momentum equation can be expressed as

$$\frac{\varepsilon \mathrm{Re}}{2\gamma Ma_{in}^2}\frac{\partial \tilde{P}_0}{\partial \tilde{x}}=\frac{1}{\tilde{r}}\frac{\partial}{\partial \tilde{r}}\left(\tilde{r}\frac{\partial \tilde{u}_0}{\partial \tilde{r}}\right) \tag{20}$$

With the boundary conditions in Eqs. (15) and (16), Eq. (20) can be integrated twice with respect to $\tilde{r}$, and then one gets

$$\tilde{u}_0(\tilde{x},\tilde{r})=-\frac{\varepsilon \mathrm{Re}}{8\gamma Ma_{in}^2}\frac{\partial \tilde{P}_0}{\partial \tilde{x}}\left(1+4\frac{2-\sigma_v}{\sigma_v}\frac{Kn_{in}}{\tilde{P}_0}-\tilde{r}^2\right) \tag{21}$$

Multiplying the above equation by $2\pi\,\tilde{r}$ and integrating once with respect to $\tilde{r}$, then multiplying it by $1/\pi\,R_0^2$, one can obtain

$$\bar{\tilde{u}}_0(\tilde{x})=-\frac{\varepsilon \mathrm{Re}}{16\gamma Ma_{in}^2}\frac{\partial \tilde{P}_0}{\partial \tilde{x}}\left(1+8\frac{2-\sigma_v}{\sigma_v}\frac{Kn_{in}}{\tilde{P}_0}\right) \tag{22}$$

Substituting Eq. (22) into Eq. (19), will yield

$$\frac{\partial \tilde{P}_0}{\partial \tilde{x}}=-\frac{16\gamma Ma_{in}^2}{\varepsilon \mathrm{Re}}\frac{1}{\tilde{P}_0+8\frac{2-\sigma_v}{\sigma_v}Kn_{in}} \tag{23}$$

Using the initial boundary conditions, $\tilde{P}_0(x)\big|_{x=0}=1$, an expression for the pressure distribution can be obtained:

$$\tilde{P}_0(x)=-8\frac{2-\sigma_v}{\sigma_v}Kn_{in}+\sqrt{\left(1+8\frac{2-\sigma_v}{\sigma_v}Kn_{in}\right)^2-\frac{64}{\mathrm{Re}}\gamma Ma_{in}^2\frac{L}{D_h}\tilde{x}} \tag{24}$$

The Fanning friction factor obtained from is given by

$$f_F(x)=\frac{16}{\mathrm{Re}}\frac{1}{1+8\frac{2-\sigma_v}{\sigma_v}\frac{Kn_{in}}{\tilde{P}_0(x)}} \tag{25}$$

The normalized Fanning friction factor (or coefficient) can be derived as

$$NC_F(x)=\frac{f_F}{16/\mathrm{Re}}=\frac{1}{1+8\frac{2-\sigma_v}{\sigma_v}\frac{Kn_{in}}{\tilde{P}_0(x)}} \tag{26}$$

Substituting the pressure distribution equation (24) and Eq. (17) into Eq (26), $NC_F$ can be written as

$$NC_F(x)=\frac{f_F}{16/\mathrm{Re}}=\frac{1}{1+\dfrac{8\frac{2-\sigma_v}{\sigma_v}\sqrt{\frac{\pi\gamma}{2}}\frac{Ma_{in}}{\mathrm{Re}}}{-8\frac{2-\sigma_v}{\sigma_v}\sqrt{\frac{\pi\gamma}{2}}\frac{Ma_{in}}{\mathrm{Re}}+\sqrt{\left(1+8\frac{2-\sigma_v}{\sigma_v}\sqrt{\frac{\pi\gamma}{2}}\frac{Ma_{in}}{\mathrm{Re}}\right)^2-\frac{64}{\mathrm{Re}}\gamma Ma_{in}^2\frac{L}{D_h}\tilde{x}}}} \tag{27}$$

So, the explicit expression of the $NC_F$ profile along the channel has been obtained with a method different from that used by Arkilic et al. [8]. As can be seen from the above equations, the local Fanning friction factor is a function of the inlet Mach number, the Reynolds number and the length-diameter ratio of the channel. And for gas flow in the microchannel at low Reynolds and Mach number ($\varepsilon << 1$, $Re \sim O(\varepsilon)$, $Ma_{in} \sim O(\varepsilon)$), the operating parameters must obey the following inequation:

$$\frac{64}{\mathrm{Re}}\gamma Ma_{in}^2\frac{L}{D_h}\tilde{x}\le\left(1+8\frac{2-\sigma_v}{\sigma_v\sqrt{\frac{\pi\gamma}{2}}\frac{Ma_{in}}{\mathrm{Re}}}\right)^2 \tag{28}$$

## 3 Results and Discussion

### 3.1 Characteristics of Gas Isothermal Flow in Microchannel

The effects of $Ma_{in}$ on the $NC_F$ profile along the microchannel for different Reynolds numbers are presented in Figs. 1 to 3. The dash lines shown in Figs. 1 and 2 are obtained from Eq. (27).

As illustrated in Figs. 1 and 2, for Re = 0.05 and Re = 10, $NC_F < 1$, the Fanning friction factor of gas flow in a microchannel is smaller than that in a circular tube with conventional size due to slip flow at the microchannel wall. Thus, rarefaction has a significant influence on the $NC_F$ profile along the microchannel. Also, $NC_F$ decreases with increasing inlet Mach numbers.

It can be seen from Fig. 1 that for small inlet Mach numbers, $NC_F$ remains constant along the streamwise direction, since variations of pressure along the axis of the microchannel are not remarkable. In the case of $Ma_{in}$= 0.001, as the pressure drops along the gas flow direction, the local Knudsen number increases. Since the influence of rarefaction effects and slip flow become more and more significant with increasing local Knudsen numbers, $NC_F$ will decrease along the channel. It is also shown in Fig. 1 that the results of numerical calculations are in good agreement with the solutions derived from Eq. (27) under the same operating conditions.

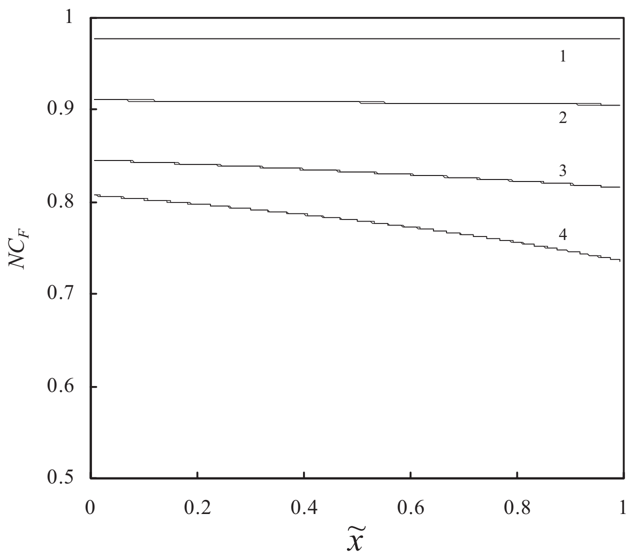


**Figure 1.** $NC_F$ of $N_2$ flows as a function of $x$ for inlet Mach numbers $Ma_{in}$. - Numerical calculation; - - - Eq. (28); Re: 0.05; $Ma_{in}$: (1) $1 \times 10^{-4}$, (2) $4.14 \times 10^{-4}$, (3) $7.68 \times 10^{-4}$, (4) $10 \times 10^{-4}$.

Fig. 2 shows that the influence of inlet Mach number values on the $NC_F$ profile along the channel at Re = 10 has the similar trends as that in Fig. 1 for Re = 0.01. However, the influence of rarefaction effects and slip flow becomes insignificant with increasing Reynolds number, and the deviation of the Fanning friction factor in the microchannel from that in a circular tube with conventional size tends to reduce as the Reynolds number increases. It is found that the results of numerical calculations are also in good agreement with those calculated from Eq. (27) for Re = 10.

The results presented in Fig. 3 show the influence of the inlet Mach number on $NC_F$ as a function of the normalized channel length for Re = 400. It is evident that the Fanning friction factor increases with increasing inlet Mach numbers.

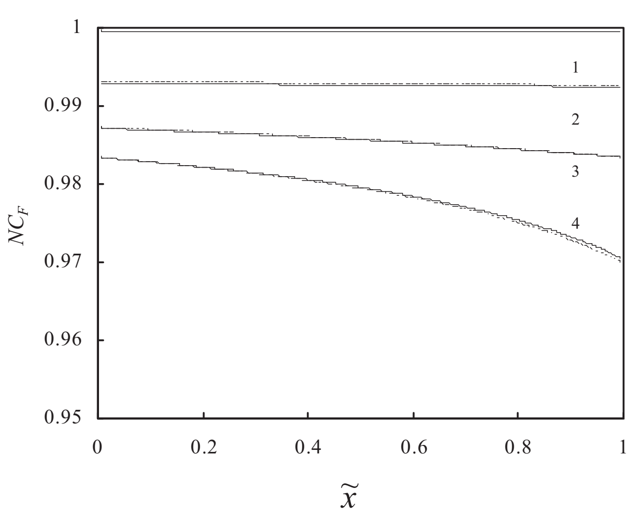


**Figure 2.** $NC_F$ of $N_2$ flows as a function of $x$ for inlet Mach numbers $Ma_{in}$. – Numerical calculation; - - - Eq. (28); Re: 10.0; $Ma_{in}$: (1) $1 \times 10^{-4}$, (2) $5.85 \times 10^{-3}$, (3) 0.011, (4) 0.014.

When the inlet Mach number is small, $NC_F$ remains constant along the channel; while for a large inlet Mach number, $NC_F$ increases along the gas flow direction. The results indicate a trend very different from the trends in Figs. 1 and 2, that is, the Fanning friction factor of gas flow in the microchannel is larger than that in conventional size tubes. These phenomena may be caused by the increase of the dimensionless velocity gradient at the wall, a result of the gas acceleration induced by compressibility of gas flow in a long microchannel [2].

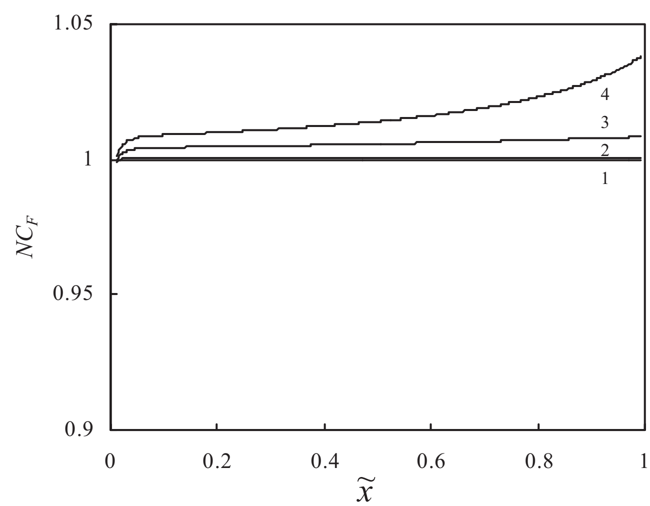


**Figure 3.** $NC_F$ of $N_2$ flows as a function of $x$ for inlet Mach numbers $Ma_{in}$. Re: 400; $Ma_{in}$: (1) $1 \times 10^{-4}$, (2) 0.037, (3) 0.069, (4) 0.09.

### 3.2 Influence of Operation Conditions on $NC_{F,out}$

It is clearly seen from Figs. 1 to 3 that the influence of the rarefaction effect and compressibility is most remarkable at the outlet of the channel. So, the normalized Fanning friction factor at the outlet of channel, $NC_{F,out}$, can be chosen to represent the influence of the rarefaction effect and compressibility on gas flow in the microchannel.

Fig. 4 shows $NC_{F,out}$ as a function of the inlet Mach number for various Reynolds numbers. As can be seen in this figure, for operating Reynolds numbers smaller than 50, $NC_{F,out} < 1$, and $NC_{F,out}$ decreases with increasing inlet Mach numbers due to more significant rarefaction effects; for operating Reynolds number larger than 50, the rarefaction effect is negligible, the gas flow in the microchannel is controlled only by compressibility, therefore $NC_{F,out} > 1$ and increases with the inlet Mach number.

Fig. 5 shows the influence of the inlet Mach number on $NC_{F,out}$ as a function of the Reynolds number. It is found that, when the inlet Mach number is lower than 0.03, $NC_{F,out}$ increases with the increase of the Reynolds number for a fixed inlet Mach number and finally approaches 1, indicating that gas flow in the microchannel is dominated by rarefaction effects at small inlet Mach number and Reynolds number conditions. However, when the inlet Mach number is

  

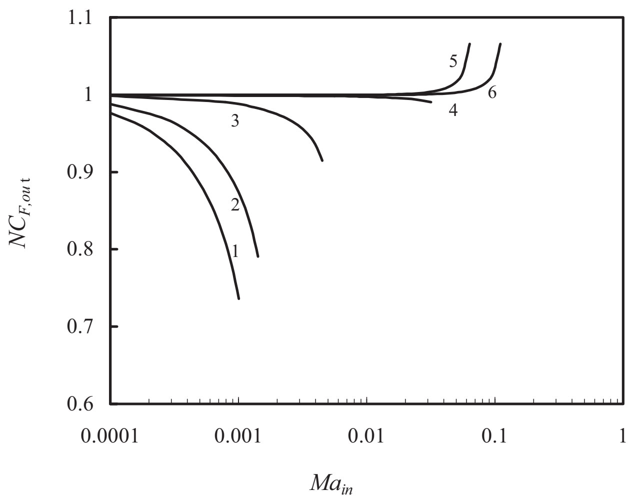


**Figure 4.** $NC_{F,out}$ of $N_2$ flows as a function of inlet Mach numbers. Re: (1) 0.05, (2) 0.1, (3) 1.0, (4) 50, (5) 200, (6) 600.

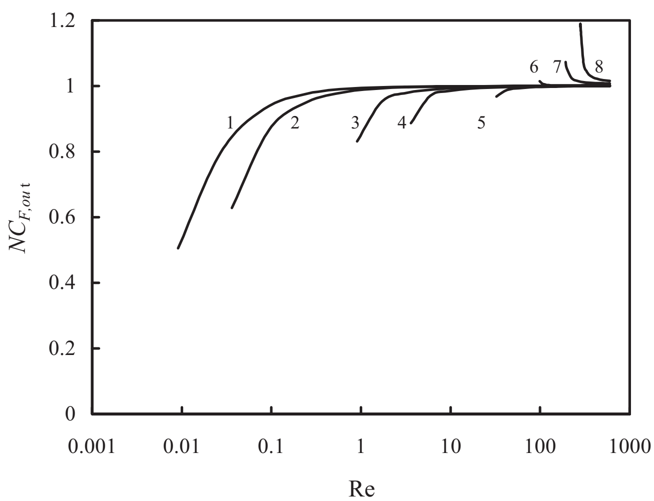


**Figure 5.** $NC_{F,out}$ of $N_2$ flows as a function of Re. $Ma_{in}$: (1) $5 \times 10^{-4}$, (2) 0.001, (3) 0.005, (4) 0.01, (5) 0.03, (6) 0.05, (7) 0.07, (8) 0.085.

greater than 0.05, $NC_{F,out} > 1$, $NC_{F,out}$ decreases and also progressively approaches one with raising Reynolds number for a fixed inlet Mach number, thus revealing that the effects of compressibility on gas flow in the microchannel are significant for large inlet Mach numbers and Reynolds numbers.

## 4 Conclusions

The effects of compressibility and rarefaction on the local flow resistance of isothermal gas flow in circular microchannels for a wide range of operating conditions have been numerically studied in detail. Two-dimensional compressible momentum equations were solved by a perturbation analysis and the PISO algorithm. The explicit expression of the $NC_F$ profile along the channel was obtained in this paper. It was found that the local Fanning friction factor is a function of the inlet Mach number, the Reynolds number and the length-diameter ratio of the channel.

For a higher Reynolds number and a larger inlet Mach number, the friction coefficient is higher than the value in macrotubes, the gas flow in the microchannel is dominated only by compressibility; while for a lower Reynolds number and a smaller inlet Mach number, the Fanning friction factor of gas flow in the microchannel is smaller than that in a circular tube with conventional size due to slip flow at the microchannel wall, clarifying that rarefaction has a significant effect on fluid flow characteristics.

## Acknowledgements

The authors gratefully acknowledge the financial support provided by the National Natural Science Foundation of China (Grant Nos. 20176057, 20122201, 20376080, 20396009) and the China National Petroleum Corporation (20396009), the Key Program for International Cooperation of Science and Technology (2001CB711203), and the Innovative project of the Dalian Institute of Chemical Physics, Chinese Academy of Sciences (No. K2003E2).

Received: October 13, 2004 [CET 7079]

## Symbols used

| | | |
|---|---|---|
| $C_F$ | [–] | Fanning friction factor, $C_F = f_F$ Re |
| $D_h$ | [m] | hydraulic diameter (= 2 $R_0$) |
| $f_F$ | [–] | Fanning friction coefficient |
| $Kn$ | [–] | Knudsen number |
| $L$ | [m] | channel length |
| $M$ | [mol·kg$^{-1}$] | gas mole mass |
| $Ma$ | [–] | Mach number |
| $NC_F$ | [–] | normalized Fanning friction factor |
| $P$ | [Pa] | pressure |
| $\tilde{P}$ | [–] | dimensionless pressure |
| Pr | [–] | Prandtl number |
| $r$ | [m] | radial coordinate |
| $\tilde{r}$ | [–] | dimensionless radial coordinate |
| $R_0$ | [m] | channel radian |
| Re | [–] | Reynolds number |
| $R_g$ | [J·mol$^{-1}$·K$^{-1}$] | gas constant |
| $u$ | [m·s$^{-1}$] | axial velocity |
| $\bar{u}$ | [m·s$^{-1}$] | axial average velocity |
| $\tilde{u}$ | [–] | axial dimensionless velocity |
| $v$ | [m·s$^{-1}$] | radial velocity |
| $\tilde{v}$ | [–] | radial dimensionless velocity |
| $x$ | [–] | axial coordinate |
| $\tilde{x}$ | [–] | axial dimensionless coordinate |

  

*Greek symbols*

| | | |
|---|---|---|
| $\rho$ | [kg·m$^{-3}$] | gas density |
| $\mu$ | [N s·m$^{-2}$] | gas viscosity |
| $\sigma_v$ | [–] | tangential momentum accommodation coefficient |
| $\varepsilon$ | [–] | channel radial/channel length |
| $\gamma$ | [–] | ratio of specific heats |
| $\lambda$ | [m] | mean free path of gas molecules |

*Subscripts*

| | |
|---|---|
| 0,1 | zero- or first-order variables for perturbation |
| in | inlet |
| wall | channel wall |

## References


[1] P. Wu, W. A. Little, *Cryogenics* **1984**, 415.
[2] Z. Y. Guo, X. B. Wu, *Int. J. Heat Mass Transfer* **1997**, *40 (13)*, 3251.
[3] J. Harley, J. Pfahler, H. Bau, J. N. Zemel, *Proc. ASME Heat Transport Proc. HTD* **1989**, *116*, 1.
[4] J. Pfahler, J. Harley, H. Bau, J. N. Zemel, *Sensors, Actuators, Systems DSC* **1991**, *31*, 49.
[5] S. B. Choi, R. F. Barron, R. O. Warrington, *Proc. ASME DSC* **1991**, *32*, 123.
[6] H. P. Kavehpour, M. Faghri, Y. Asako, *Numer. Heat Transfer, Part A*, **1997**, *32*, 67.
[7] C. S. Chen, S. M. Lee, J. D. Shen, *Numer. Heat Transfer A*, **1998**, *33*, 749.
[8] E. B. Arkilic, M. A. Schmidt, K. S. Breuer, *J. Microelectromech. Syst.* **1997**, *6 (2)*, 167.
[9] A. H. Shapiro, *The Dynamics and Thermodynamics of Compressible Fluid Flow,* John Wiley & Sons, New York **1953.**
[10] Wenquan Tao, *Advance in Numerical Heat Transfer,* The Science Press, Bei Jing **2000**.